

Robustness of the Thirty Meter Telescope Primary Mirror Control System

Douglas G. MacMynowski^a, Peter M. Thompson^b, Chris Shelton^c and Lewis C. Roberts, Jr.^c

^aCalifornia Institute of Technology

Department of Control and Dynamical Systems, Pasadena CA 91125

^bSystems Technology, Inc., Hawthorne, CA 90250

^cJet Propulsion Laboratory, California Institute of Technology, Pasadena, CA 91109

ABSTRACT

The primary mirror control system for the Thirty Meter Telescope (TMT) maintains the alignment of the 492 segments in the presence of both quasi-static (gravity and thermal) and dynamic disturbances due to unsteady wind loads. The latter results in a desired control bandwidth of 1 Hz at high spatial frequencies. The achievable bandwidth is limited by robustness to (i) uncertain telescope structural dynamics (control-structure interaction) and (ii) small perturbations in the ill-conditioned influence matrix that relates segment edge sensor response to actuator commands. Both of these effects are considered herein using models of TMT. The former is explored through multivariable sensitivity analysis on a reduced-order Zernike-basis representation of the structural dynamics. The interaction matrix (“*A*-matrix”) uncertainty has been analyzed theoretically elsewhere, and is examined here for realistic amplitude perturbations due to segment and sensor installation errors, and gravity and thermal induced segment motion. The primary influence of *A*-matrix uncertainty is on the control of “focus-mode”; this is the least observable mode, measurable only through the edge-sensor (gap-dependent) sensitivity to the dihedral angle between segments. Accurately estimating focus-mode will require updating the *A*-matrix as a function of the measured gap. *A*-matrix uncertainty also results in a higher gain-margin requirement for focus-mode, and hence the *A*-matrix and CSI robustness need to be understood simultaneously. Based on the robustness analysis, the desired 1 Hz bandwidth is achievable in the presence of uncertainty for all except the lowest spatial-frequency response patterns of the primary mirror.

Keywords: Extremely Large Telescopes, Control Systems, Uncertainty

1. INTRODUCTION

The primary mirror (M1) of the Thirty Meter Telescope (TMT) is composed of 492 hexagonal segments (Fig. 1), with the out-of-plane degrees of freedom controlled by the primary mirror control system (M1CS). There are two control loops within M1CS. A global control loop maintains the position of the mirror segments, using feedback from edge sensors that measure the relative motion between neighbouring segments. A local servo control loop using feedback of the actuator displacement provides the required stiffness at low frequency. The control approach is broadly similar to that used at the Keck Observatories.^{1,2} However, there are several key differences that are important in evaluating the robustness to uncertainty.

First, while the Keck control system compensates only for low frequency disturbances such as thermal variations or the changing orientation of the mirror with respect to gravity, the TMT M1CS will also compensate for some wind-induced motion of the M1 segments. This results in a higher bandwidth requirement (see [3, 4]), which in turn leads to the potential for control-structure-interaction (CSI)^{5,6}: undesirable dynamic interaction between the primary mirror control system and the (uncertain) telescope structural dynamics. This issue has been discussed earlier,⁷⁻¹⁰ and needs to be addressed both for local actuator servo loops and global M1CS feedback; this paper updates the previous analysis based on current TMT actuator designs.

A second issue is that the control system relies on knowledge of the interaction matrix, or *A*-matrix, that relates actuator commands to sensor response.¹¹ The condition number of this matrix scales with the number of segments, and thus robustness to small errors has the potential to be a much larger challenge for larger telescopes than at Keck. A detailed theoretical analysis is given in [12], and simulation results are presented herein. Both robustness topics need to be considered together, as a control system robust to either uncertainty in isolation might not be robust to simultaneous uncertainty in both the dynamics and the interaction matrix.

TMT has considered both “soft” (voice-coil) and “hard” (e.g. piezoelectric) actuators,¹³ and the analysis here focuses primarily on the selected voice-coil actuator design. The unsteady forces on the mirror segments due to wind turbulence within the enclosure lead to requirements both on the M1CS control bandwidth, of roughly 1 Hz,^{3,4} and also on the low-frequency stiffness of the M1CS actuators, and hence on the servo loop gain. While both the local (actuator servo) and global position control loops would be straightforward to design if the segments were supported by a rigid backplane, the flexibility of the mirror cell and telescope structure lead to coupling between the segments that can potentially lead to instability. The key insight relevant to analysis is that a diagonal system of identical subsystems is diagonal under any change in basis, and thus the dynamics of the 492 segments and their control can be projected onto a Zernike basis.^{7,8} Since the structure is stiff on short length-scales, CSI robustness is only a concern for the lowest spatial frequencies, or equivalently, the lowest Zernike bases.

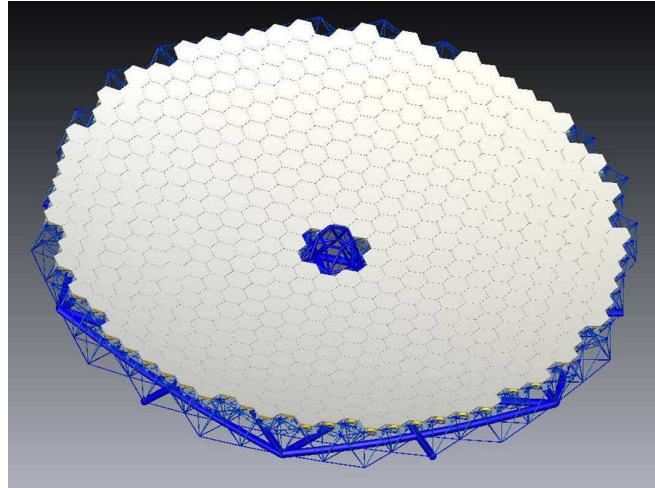


Figure 1. TMT primary mirror, composed of 492 hexagonal segments mounted on a flexible mirror cell.

The second source of uncertainty relevant to M1CS robustness is errors in the interaction matrix (A -matrix) between the edge sensors and the segment actuators. The TMT edge sensors are sensitive to a linear combination of inter-segment height differences and the dihedral angle between neighbouring segments (eq. (6)). The ratio of these sensitivities is denoted L_{eff} , with units of length (an effective moment arm). The dihedral sensitivity makes focus-mode observable. The nominal L_{eff} for segment-edge-mounted sensors on TMT is less than half the value at Keck, and also varies with the inter-segment gap. The condition number of A scales with the number of segments and inversely with L_{eff} , making sensitivity to errors in A a factor of 40 larger than at Keck. Analysis¹² demonstrates that there should be sufficient *stability* robustness to gain errors (including variations in L_{eff}), and high sensitivity only to “geometry” errors that affect all elements of the A -matrix independently (e.g. sensor installation errors). However, while stability is guaranteed for gain errors, performance can still suffer, as L_{eff} can change by as much as $\pm 35\%$ due to segment gap changes that are a function of segment installation errors, zenith angle, and temperature.

Simulations have therefore been conducted to evaluate the actual robustness to realistic predicted perturbations. The results are consistent with the analysis. Based on these simulations, we conclude that the effects of A -matrix uncertainty can be managed so that this is not a significant challenge to M1CS stability. However, we will have to take straightforward steps to manage the effects that the uncertainty has on performance. In particular, we will (i) use gap-compensated sensor measurements so that the height-sensitivity of the sensor output is (almost) insensitive to gap, and (ii) update the A -matrix and its pseudo-inverse B periodically in order to compensate for the variation in sensor dihedral sensitivity with gap.

In addition, it may be necessary to measure the A -matrix elements whenever new segments are installed (to manage the sensitivity to sensor installation tolerances). The simulations suggest that this third step can be avoided and that the A -matrix updates can be based on the analytically computed functional dependence on gap. For a gap-compensated capacitive sensor, the A -matrix update should occur roughly every $3\text{-}5^\circ$ of zenith angle change or 10°C temperature change.

The next section evaluates CSI for the servo and global loops, followed by A -matrix analysis in Sec. 3. The simultaneous combination of the uncertainties is discussed in Sec. 3.5.

2. CONTROL STRUCTURE INTERACTION

2.1. Preliminaries

It is clear that a control system that is designed assuming that a segment is mounted on a rigid support can lead to problems if the segment is actually mounted on a flexible structure. While TMT has many more segments than Keck, in previous papers, we demonstrated that the CSI risk scales with the ratio of the total mass of

controlled segments to the mass of the mirror cell,^{7,8} because it is the total mass of controlled segments that determines the net force introduced into the coupling structure. That is, increasing the number of controlled segments does not affect stability if the areal density remains constant; it is the desire for increased bandwidth that leads to the requirement to analyze CSI in more depth for TMT.

A natural basis for exploring robustness would be in actuator space. However, there is both a computational motivation and an interpretive value if we instead project the dynamics onto a Zernike basis.* Note that any structural mode will project onto multiple basis vectors (though there is often a dominant one or two), and conversely, any basis vector will include dynamics associated with multiple modes, and thus multivariable analysis is still required. If we included the first 492 Zernike basis vectors, there would be no computational savings relative to the original untransformed system. However, the advantage in using the Zernike basis is that stability characteristics can be accurately predicted with relatively few basis vectors included. This results from the fact that the coupling, and therefore the control-structure-interaction, is dominated by the most compliant, lowest frequency modes of the supporting structure, and these are the longest wavelength, lowest wavenumber modes, and predominantly project onto the lowest order Zernike basis vectors. For high wavenumber motion involving significant relative motion between neighbouring segments, the support structure is relatively stiff.

All analyses herein will be presented for a 30° zenith angle. The structural damping is assumed to be 0.5%. In order to maintain adequate detail on the dynamics of each segment, the segment dynamics are not included in the overall telescope model, but are added in as needed, thus even the segment dynamics are projected onto the Zernike basis. Other analysis details are given in [7], including the projection of the telescope structural dynamics onto a Zernike basis and verification that the structural compliance is largest at low wavenumber. At sufficiently high wavenumber, the mirror cell response is dominated by the purely local compliance of the top layer, which does not introduce any coupling between segments.

The multivariable robustness metric used here is to require the peak magnitude (H_∞ norm) of the sensitivity to be less than about 2; this is a reasonable margin in the absence of a specific understanding of the structure and magnitude of the uncertainty (see e.g. [14] for further details). If the structure and segment dynamics transfer function is $G(j\omega)$ and the controller is $K(j\omega)$, then the robustness margin requirement is:

$$\|S\|_\infty = \max_{\omega} \bar{\sigma}(S(j\omega)) \leq 2 \quad \text{where} \quad S = (1 + GK)^{-1} \quad (1)$$

and $\bar{\sigma}(j\omega)$ is the maximum singular value of the transfer function matrix. For the servo loop, $G(s)$ is the transfer function from actuator force input to the output of a collocated encoder, while for the global loop, it is from the position command to the actuator servo loop to the segment position estimated from edge sensors.

2.2. (Local) Servo loop

While much of the underlying analysis techniques are the same, actuator and actuator servo designs have been updated significantly since [7]; see [13]. The TMT actuator uses a voice-coil, with significant passive damping added in parallel, and encoder feedback that is (nearly) collocated with the force input. The open-loop transfer function for the actuator is shown in Fig. 2, both for a segment mounted on a rigid-base, and for segments mounted on the mirror cell, with the dynamics projected onto the first three low-order Zernike basis functions (piston, tip, tilt). The actuator damping makes the open-loop segment resonance (at ~9 Hz) heavily damped, and also adds some damping to any mirror cell resonances that couple with the actuator motion.

Because the servo sensor and actuator are nearly collocated, the transfer function between the actuator command and output will be phase-bounded regardless of the structural dynamics and mirror cell coupling (i.e. positive-real transfer function from force to velocity). This property is valid up to at least 150 Hz, based on measurements on a prototype actuator and segment support assembly; improved designs should maintain collocation up to higher frequencies. An appropriate phase-bounded control strategy can thus guarantee stability regardless of knowledge of the coupling. CSI can thus be divided into three frequency regions:

- Integral gain is required at low frequencies for adequate stiffness; phase-bounded arguments therefore cannot be used to guarantee stability here, but the finite element model should be accurate enough at low frequencies (below ~15 Hz) to predict the multivariable sensitivity needed to evaluate robustness.

*We orthonormalize each higher mode relative to lower order modes at the segment locations, so the resulting basis is not precisely a Zernike basis.

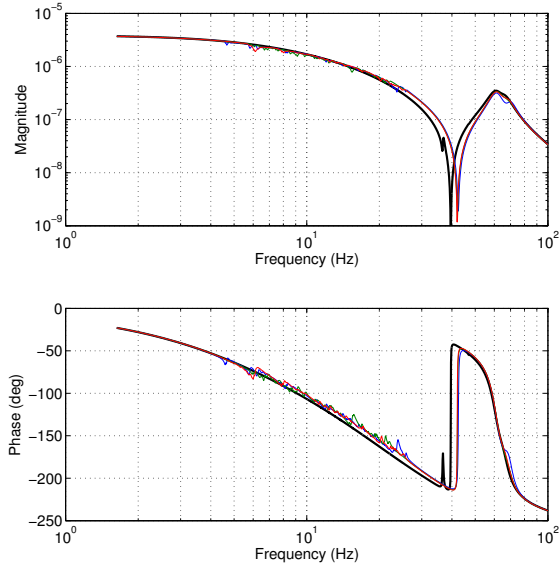


Figure 2. Open-loop actuator transfer function for segment mounted on rigid base (black, thick line) and for segment dynamics on mirror cell, projected onto global piston, tip and tilt.

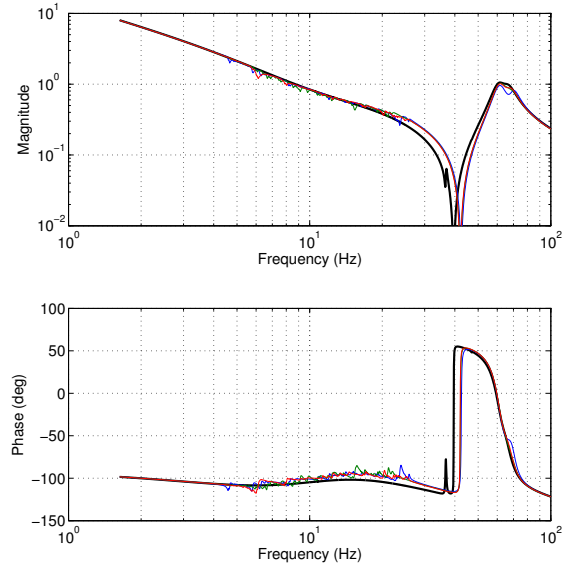


Figure 3. Loop transfer function for actuator servo, line styles as Fig. 2. The phase margin on a rigid base is 75° and the gain margin above 150 Hz exceeds 12 dB.

- Between ~ 15 Hz and ~ 150 Hz, if the controller is appropriately phase-bounded, then stability is guaranteed regardless of coupling, with zero risk. If a gain-stable control approach were used instead, then the CSI risk would need to be evaluated based on models; since the FEM may not be accurate in this frequency region, there would be some risk to this approach.
- Above ~ 150 Hz, the system cannot be guaranteed to be phase-bounded due to non-collocation, and the controller must be gain-stable with sufficient gain-margin to accommodate a highly uncertain plant.

The model-based loop transfer function for the actuator servo is shown in Fig. 3; the servo has also been evaluated on prototype hardware and verified to have at least 10 dB gain margin above 150 Hz. The compensator is appropriately phase-bounded above 10 Hz to guarantee stability regardless of unknown structural dynamics.

The multivariable sensitivity function is shown in Fig. 4; this verifies robustness to uncertainty below ~ 10 Hz where the compensator phase is not sufficient to guarantee stability. Note that SISO analysis for each basis vector separately shows no sign of significant structural coupling (see Fig. 3), while there is clearly significant multivariable coupling, indicating that multivariable analysis is essential. The results in Fig. 4 were computed with 2000 structural modes and the first 45 Zernike basis functions, however, the results are essentially identical with as few as 10 basis functions; this represents a substantial computational savings relative to computing the sensitivity with all 492 segments. Note that even though the M1 piston, tip and tilt (Zernike radial degree 0 and 1) deflections are unobservable in the global control loop, forces on the mirror aligned with these basis functions will excite the servo loop, which must still be stable when coupled to the telescope structure. The peak sensitivity of 2.1 for this servo design is at 5.8 Hz, and corresponds to structural modes that project almost entirely onto these basis functions; the peaks between 8 and 10 Hz are mostly due to radial degree $p = 2$ modes.

As noted, TMT has also evaluated several hard actuator technologies. These also require a servo loop, but the requirements are less demanding as less gain is required to provide adequate low frequency stiffness. However, while the voice-coil actuator naturally provides damping at the segment resonant frequencies, a hard actuator would require an additional force-feedback loop to provide damping, and the CSI robustness issues associated with this higher bandwidth loop are comparable to those of the soft actuator.

2.3. Global control

The global primary mirror control loop uses edge sensors to estimate the position of each mirror segment at the actuator locations, and collocated SISO control loops to minimize the mirror motion. The global control can

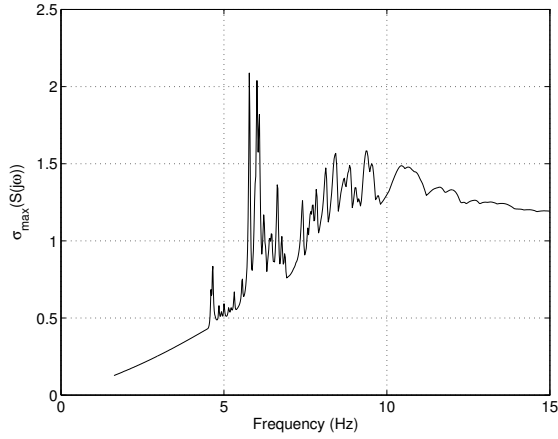


Figure 4. Multivariable sensitivity for actuator servo loop.

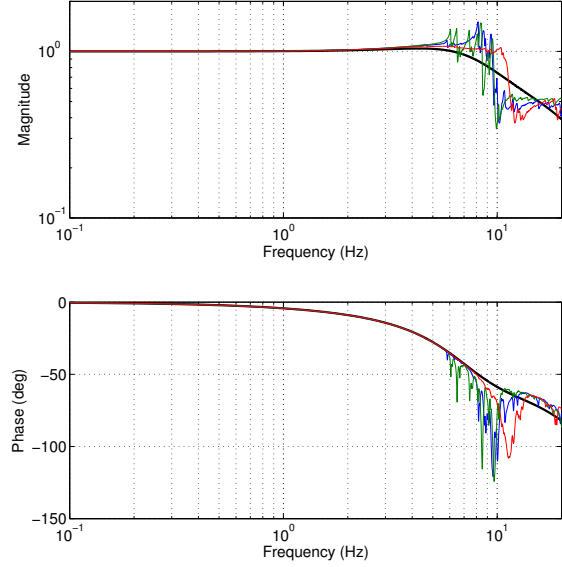


Figure 5. Open-loop transfer function for global M1CS control loop, line styles as Fig. 2.

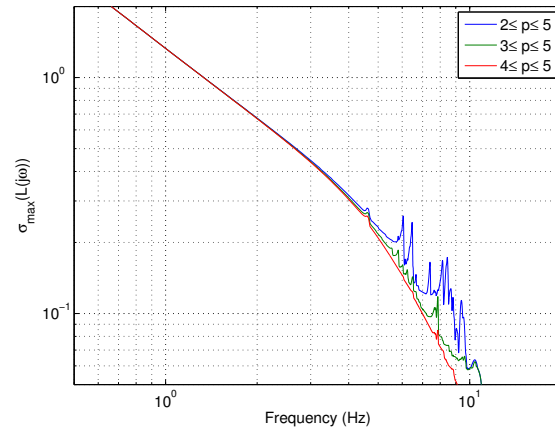
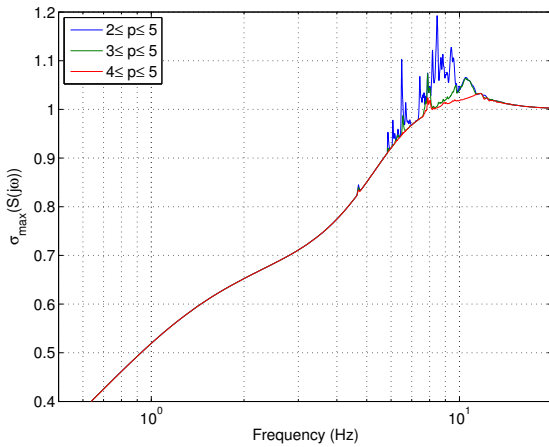


Figure 6. Maximum singular value of sensitivity (left) and principal loop gain (right) for the global M1CS control loop at a 1 Hz bandwidth, projected onto different Zernike basis functions. Only radial degree 2 (focus and astigmatism) have any significant CSI effect at this bandwidth.

also be analyzed in a Zernike basis. It is also straightforward to use a modal control approach by transforming the segment position estimates \hat{x} into either Zernike space or the (similar) basis resulting from the singular value decomposition of the influence matrix. The open-loop transfer function from a position command for an actuator servo to the mirror surface response at that actuator is shown in Fig. 5, both for a segment mounted on a rigid base, and segments mounted on the mirror cell and projected onto low order Zernikes.

The Keck global M1CS loop used pure integral control since only a low bandwidth was required. Since the bandwidth is limited by the gain-margin from lightly damped structural modes at frequencies well above the control bandwidth, significantly higher bandwidths can be achieved by adding roll-off to the compensator.⁷ A second order Butterworth filter is used with corner frequency a factor of 5 higher than the desired bandwidth.

The multivariable sensitivity and principal loop gain (maximum singular value of the loop transfer function) are shown in Fig. 6 for a 1 Hz control bandwidth. At this bandwidth, the peak sensitivity is less than 1.2, and the peak loop gain above 5 Hz is 0.26. Different Zernike modes are projected out separately in the Figure, to illustrate that the largest constraint is on the lowest radial-degree Zernike modes. For focus-mode, robustness to

A -matrix error suggests a 12 dB gain margin requirement, but even so, a 1 Hz bandwidth could be acceptable; a lower bandwidth is likely to be used due to sensor noise propagation. From this CSI analysis, Zernike modes above radial degree $p = 2$ could be controlled with a bandwidth of 2 Hz or higher.

3. INTERACTION MATRIX UNCERTAINTY

The edge sensor output can be related to the displacement of the mirror surface at the actuator locations by

$$y = Ax \tag{2}$$

(ignoring noise); the A -matrix can be computed from geometry. The displacement estimate \hat{x} at the actuator locations uses the pseudo-inverse, $B = \lim_{\rho \rightarrow 0} (A^T A + \rho I)^{-1} A^T$, so that $\hat{x} = (BA)x$ (plus noise). If the matrix B is computed from the correct A matrix, then $BA = I$ for all observable directions (i.e. excluding global piston/tip/tilt). However, in general, errors or temporal variations in A means that $BA \neq I$, and if the errors are sufficiently large, then decreased performance or possible instability of the M1CS global control loop can result. We start by considering general criteria for stability- and performance-robustness, and then present simulation results with predicted TMT perturbations.

3.1. Stability robustness

Errors in the A -matrix can be divided into the following categories:

- Actuator gain errors; these are the same for every element in a given column of the A -matrix,
- Sensor gain errors; these are the same for every element in a given row,
- Dihedral gain error; also the same for every element in a given row, however, rather than the entire row changing by a scale factor, only the ratio of dihedral and height sensitivity for the sensor are changed, or
- “Geometry” errors, in which every non-zero element of the A -matrix can vary independently.

Variations in sensor gain with gap (or shear, or temperature), or variations between sensors or actuators in their frequency response, all fit into the first few categories, while sensor installation tolerances and some of the effects from segment installation tolerances can lead to the final category of perturbations.

Ref. [12] uses small-gain analysis to demonstrate stability-robustness to order-one errors associated with the first three sources above. μ -analysis (structured singular values) is used to demonstrate that there can be extreme sensitivity to the fourth category of error. Robustness to actuator and sensor gain errors is consistent with intuition; a change in actuator gain simply means a change in the bandwidth with which that particular segment displacement will converge. Thus actuator and sensor gain errors consume some fraction of the gain margin of the control system, and should ideally be kept to $\sim 10\%$. In an ideal setting of perfect integral control, there is infinite gain margin, and instability only occurs if the gain changes by a fraction of more than one, i.e. if it can change sign. (Note that from Fig. 6 the gain margin based on CSI considerations is a factor of 4.) Robustness to variations in the relative dihedral and height sensitivity of the sensors is not immediately apparent. However, because the dihedral sensitivity only has a significant effect on focus-mode, and the height sensitivity does not affect focus-mode, the measurement of focus-mode is essentially decoupled from the rest of the control problem, and variations in dihedral sensitivity affect stability of focus-mode control in the same way that variations in sensor gain affect the overall control problem. (This does not imply that the performance is not affected; this will be discussed shortly.)

All of the gain errors are extremely structured in how they affect the A matrix (1476 or 2772 unknown parameters out of 16632 non-zero values). If, however, every non-zero element of the A -matrix can vary independently, then stability-robustness can become a significant problem. To guarantee that perturbations cannot lead to instability, the errors in A -matrix entries must be less than of order one part in 10^4 . This sensitivity scales linearly with the number of segments, and inversely with L_{eff} , which is why this was not a problem at Keck; the corresponding sensitivity there is a factor of ~ 40 lower. Note that this sensitivity for TMT corresponds to sensor installation tolerances of order $100\mu\text{m}$ or so (based on actuator-sensor distances of order 1 m). Thus there is no reason to expect stability problems associated with this type of error for TMT. Furthermore, the particular pattern of errors in the A -matrix entries that leads to instability is not likely; ref. [12] estimates that the uncertainty bound that gives a 95% probability of stability is of order 100 times less severe than that required to guarantee stability. (Although this also implies that we should be careful not to be overconfident in simulations of sensor installation error, as it is difficult to assign an overall probability of stability from a small number of simulations.)

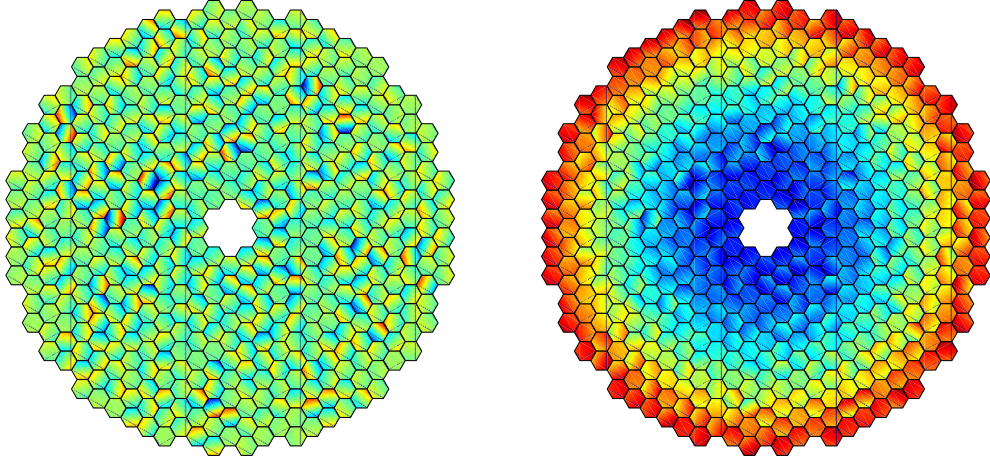


Figure 7. Example of estimation errors due to ill-conditioning (here due to one realization of random segment installation errors). The actual displacement pattern on the left results in the estimated displacement pattern on the right, which consists primarily of the actual pattern, plus an erroneous additional focus-mode component that is roughly 5 times larger.

3.2. Performance robustness

While the analysis summarized above describes what types of uncertainty have the potential to lead to instability, it is essential to understand the effects of the specific structure of uncertainty that will be encountered at TMT, and to relate the generic effects described above to representative specific perturbations in operational parameters. The list of perturbations simulated is discussed in the next subsection. For each perturbation, the pseudo-inverse B is computed from the nominal configuration, and the significance of the deviation between the nominal and perturbed A -matrix computed as follows

With an integral control law, then in discrete-time, the closed-loop dynamics (ignoring CSI) are

$$x_{k+1} = (I - \alpha BA)x_k \quad (3)$$

with $0 < \alpha < 1$. In the absence of any structural dynamics, a sufficient condition for stability is for the spectral radius $\rho(I - BA) < 1$. However, in order to better capture not simply the stability boundary but the degradation in performance relative to the ideal case, a better measure of the error is to look at the worst-case estimator error, given by the maximum singular value:

$$J = \max_{\|x=1\|_2} \|\hat{x} - x\|_2 = \sigma_{\max}(I - BA) \quad (4)$$

This is the induced-norm of the matrix, giving the maximum ratio of rms estimator error to rms displacement.

Small values of $\sigma_{\max}(I - BA)$ guarantee good performance, but larger values do not necessarily imply a problem; if $\rho(I - BA)$ is small the system is not only stable but will rapidly converge. The ratio between these two metrics can be arbitrarily large; consider the case of a matrix $M = ab^T$ where vectors a and b are orthogonal: the eigenvalues of M are zero but the maximum singular value is not. This matrix is non-normal, and for this type of matrix the transient response to initial conditions may increase before eventually decaying. This situation does occur in the simulation results; a pattern of segment motion nearly orthogonal to focus-mode can be interpreted by the estimator as focus-mode, resulting in an initial increase in focus-mode amplitude before that decays under control. The worst-case magnitude of this non-normal growth can be estimated as

$$J_{NN} = \max_k \{\sigma_{\max}[(I - BA)^k]\} \quad (5)$$

However, in simulations, time-step $k = 1$ typically leads to the worst magnification, and hence we use J in eq. (4) rather than J_{NN} to evaluate performance.

In practice, all of the maximum estimation errors reported in the next section are associated with some non-focus-mode pattern (“P1”) leading to an erroneous estimated focus-mode error; see Fig. 7 for an example

from the simulation results. The resulting impact of the error is small for two reasons. First, the focus-mode control bandwidth is expected to be significantly lower than that of all other degrees of freedom, because of higher sensor noise and less stringent performance consequences. Thus higher-frequency residual fluctuations in P1 do not lead to as large a focus-mode response as implied by the size of the estimation error. Because of the higher bandwidth on P1, the low-frequency fluctuations in P1 that the focus-mode control would respond to will be adequately controlled. Second, even with 100% estimation error, then if the residual amplitude of the pattern P1 that leads to an erroneous estimate is only a few nm, then the erroneous component of the focus-mode amplitude will only be a few nm; this is clearly tolerable. The impact on performance is borne out by time-domain simulations in which estimation errors of even 200% produce relatively small performance errors. Nonetheless, since straightforward steps can be taken to significantly reduce the estimation error, it is not necessary to operate the system with these types of errors. Keeping estimation errors below 50% also simplifies the analysis of robustness to simultaneous dynamic (CSI) and A -matrix uncertainty.

3.3. Simulation of A -matrix errors

We now turn to the simulation of specific A -matrix variations for TMT. TMT sensors are mounted to the edges of the segments, and the differential capacitance response measurement R is related to the change in height between segments z and the dihedral θ_x as

$$R = \frac{f}{y} \left(z + \frac{g}{y} \theta_x \right) \quad (6)$$

where y is the gap between sensor faces (this is also measured by the sensor), and the constants f and g depend on the design. A gap-compensated sensor output can be used instead, so that

$$R^* = z + \frac{g}{y} \theta_x \quad (7)$$

This gap-compensated output will be assumed throughout, as it reduces the variation in A significantly. However, as gaps change, then the effective moment arm $L_{\text{eff}} = g/y$ (ratio of dihedral to height sensitivity) changes. An inductive sensor has also been evaluated; its gap dependence was weaker, but the same issue arises. Over the range of temperature, zenith angle and segment installation errors, the gap between sensor faces will vary over the range 4.5 ± 1.2 mm.

Simulated A matrices have been constructed to explore the effects of segment and sensor installation tolerances, temperature, and zenith angle. The following cases have been run:

- Baseline: zero segment or sensor installation error, 30° zenith angle
- Zenith angles of 60° , 50° , 35° , 25° , 15° and 0°
- Temperature change of $\pm 5^\circ\text{C}$
- Segment installation error (see below)
- Sensor installation errors (Gaussian, standard deviation specified):
 - z error of 10 and $100 \mu\text{m}$
 - θ_x error of 0.1 and 1.0 mrad
 - θ_y error of 0.1 and 1.0 mrad

The segment installation errors are zero mean with standard deviation in x and y of $200 \mu\text{m}$ and clocking of $285 \mu\text{rad}$, and drawn from a Gaussian distribution but bounded at two standard deviations to avoid the small probability of unrealistically large errors. Note that the effect on the A matrix due to changes in temperature, zenith angle, and segment installation errors is due to the gap and resulting L_{eff} changes. This was verified by comparing these cases for an ideal sensor where the height and dihedral angle sensitivity do not change with gap.

At Keck, the B matrix is computed from an idealized A -matrix corresponding to a flat mirror with regular hexagonal segments. To understand how additional realism affects the results, cases were also run for a flat mirror with either regular hexagonal segments or the actual segment geometry.

The metric $J = \sigma_{\text{max}}(I - BA)$ is shown in Table 1. The worst-case singular value always corresponds to an output pattern of focus-mode, though the input pattern that leads to this varies. J is also shown for the

| Case type | Perturbation | Fixed A and B | | updated A and B |
|---------------------------------|------------------------------|-------------------|---------------|------------------------|
| | | focus-mode | no focus-mode | |
| Verification | flat, regular | 0.75 | 0.07 | - |
| | flat, hex | 240 | 240 | - |
| Zenith angle change | 0° | 4.4 | 0.92 | 0.4 |
| | 15° | 2.3 | 0.47 | 0.21 |
| | 25° | 0.85 | 0.17 | 0.08 |
| | 35° | 0.9 | 0.18 | 0.08 |
| | 50° | 3.6 | 0.71 | 0.31 |
| | 60° | 5.5 | 1.1 | 0.46 |
| Temperature change | -5°C | 0.3 | 0.056 | - |
| | +5°C | 0.28 | 0.053 | - |
| Segment installation error | | 4.9 | 1 | 0.43 |
| Sensor installation error | $dz = 100 \mu\text{m}$ | 0.005 | 5e-5 | - |
| | $d\theta_x = 1 \text{ mrad}$ | 0.05 | 0.015 | - |
| | $d\theta_y = 1 \text{ mrad}$ | 0.006 | 0.002 | - |

Table 1. Worst-case estimation error $J = \sigma_{\max}(I - BA)$ for different cases, with zenith angle of 30° as the baseline case for computing B . “Verification” cases test the difference between the true segment geometry on a curved surface and simplifications, the remaining cases correspond to representative variations expected in operation. The goal is to keep all values below $J = 0.5$.

case where focus-mode is not controlled; here the worst-case singular value corresponds to astigmatism. The final column simulates the prediction of A and B based on gap information, and will be discussed shortly. The following conclusions can be drawn from the table:

1. The difference between hexagonal and actual segment shapes is significant (this is relevant if analytically computed A matrices are used); the difference between flat and curved is relevant but less critical.
2. The errors are substantially reduced if focus-mode is projected out of the control.
3. Performance is not sensitive to sensor installation errors; these are small enough that the resulting “geometry” errors in A are sufficiently small to guarantee stability.
4. Gap-compensated sensing is essential to reduce the sensitivity to zenith angle variation to a more manageable level; the results for uncompensated sensors were computed but are not shown.
5. In order to keep the estimation errors below 50%, updating the A -matrix and recomputing B is required to compensate for changes in A with zenith angle and temperature.
6. This update should occur every $\sim 3^\circ$ zenith angle change and every $\sim 8^\circ\text{K}$ for temperature changes. The gap-dependence with an inductive sensor is smaller, requiring less frequent updates. If focus-mode is not corrected, updates would still be required, though less frequently.
7. Measurement of the A -matrix is not required to account for segment installation error, provided that the A matrix is computed from the measured gaps.

3.4. Updating A

Each entry in the A -matrix in eq. (2) is of the form

$$A_{ij} = (A_z)_{ij} + (A_\theta)_{ij} \quad (8)$$

corresponding to the two terms in eq. (6). Both A_z and A_θ can be determined from geometry. A and B can thus be updated using gap information, using a model for each row of A of the form $A = A_z + A_\theta(y_0/y)$ where A_z is independent of gap (height sensitivity) and A_θ (dihedral sensitivity at nominal gap) describes the dependence on the sensor gap. The final column in Table 1 is constructed by using two A matrices and sets of gap information

to estimate A_z and A_θ , and using the gap information for the other cases to predict the corresponding A . The estimation metric J is computed as before, but using the predicted pseudo-inverse B rather than baseline. The accuracy of this is limited by (i) whether the gaps for the cases used to construct A_z and A_θ change; this is only an issue if the A matrices are obtained from measured data rather than analytically, and (ii) the accuracy of the gap measurement; 1 micron is assumed herein. The calculations in Table 1 are obtained using the A matrices corresponding to $\pm 5^\circ\text{C}$ temperature shifts; this guarantees that all gaps have changed, but is limited in the accuracy of computing A_θ since the gap changes are not large compared to the gap resolution. If the prediction were based on analytical calculations (so the constant and first-order terms in the A matrix were known exactly), then this source of error would disappear. The table thus provides a conservative upper bound on the errors that will remain with this prediction strategy.

3.5. Interaction with CSI

The peak sensitivity or peak principal loop gain requirements on the global M1CS loop are the multivariable equivalents of gain margin (the former captures the effects of simultaneously gain and phase variation, the latter ensures small gain regardless of phase). The uncertainty in the A -matrix introduces an additional source of variability in the gain.

The actual variation in the gain of focus-mode due to A -matrix variation and uncertainty may be quite small, and thus the interaction between these two sources of uncertainty may not be significant. However, this does not provide a rigorous proof of stability in the multivariable case. Instead, note that the system loop gain is the product of the gain matrix BA due to estimation (ideally the identity, aside from unobservable modes) and the frequency-dependent transfer function gain computed for $BA = I$. The estimation error J computed for A -matrix uncertainty provides a norm bound on the maximum deviation of the norm of BA relative to one, while the principal loop gain calculated in Sec. 2.3 is a norm on the frequency-dependent part of the system loop gain. Because norms are sub-multiplicative, then the overall stability robustness to the combined uncertainty can be quantified. An estimation error $J < 0.5$ combined with a loop gain less than 0.5 guarantees stability, while the loop gain should be less than 0.25 to retain 6 dB gain margin against other sources of uncertainty. Because the estimation error is dominated by focus-mode effects, then the reduced gain-margin requirement for CSI only needs to be applied to focus-mode.

4. CONCLUSIONS

There are two sources of uncertainty that need to be taken into account in evaluating the robustness of M1CS. Dynamic uncertainty due to control-structure-interaction (CSI) influences both local actuator servo loops and the global (edge-sensor feedback) loops, while interaction matrix uncertainty only affects the global loop. CSI is efficiently analyzed in a Zernike basis, since it is only the lowest spatial frequencies that have any significant coupling through the telescope structure. The effects of A -matrix uncertainty are evaluated with representative perturbations.

The TMT segment actuators require a servo loop from collocated encoder feedback to provide adequate low frequency stiffness; this feedback is shown to be robust to CSI. Positivity is used to guarantee stability above 10 Hz, while model-based analysis is used to ensure that the peak multivariable sensitivity below this frequency is less than ~ 2 .

A 1 Hz M1CS global control bandwidth can be robustly achieved in the presence of CSI. Because A -matrix errors result in gain uncertainty in focus-mode in particular, a larger gain-margin and thus smaller bandwidth is required for focus-mode; this does not have any significant performance implications.

Uncertainty in the M1CS A matrix can be managed by (i) using gap-compensated sensors that eliminate the sensor height sensitivity variation with gap using local gap measurements, (ii) updating A and recomputing the pseudo-inverse B based on local gap measurements to account for the dihedral sensitivity variation; this is required roughly every 3° of zenith angle variation, and (iii) providing the capability to measure the A -matrix initially and with any segment replacement. The final step does not appear to be necessary based on the simulations conducted herein. The first two steps are needed both to guarantee stability in the presence of simultaneous uncertainty in dynamics (CSI) and in the A -matrix, and to ensure acceptable performance. It may be possible to retain acceptable performance without updating A with zenith angle, as maximum estimation errors of 200% have been simulated without significant performance loss; nonetheless, this seems like an appropriate precautionary step to take.

Acknowledgements

The finite element models used herein for the telescope structure and the primary segment assembly were developed by DSL and by HYTEC Inc., respectively. The soft actuator parameters used here are based on a design and prototype from Marjan Research. The contributions of all of these organizations are gratefully acknowledged.

The TMT Project gratefully acknowledges the support of the TMT partner institutions. They are the Association of Canadian Universities for Research in Astronomy (ACURA), the California Institute of Technology and the University of California. This work was supported as well by the Gordon and Betty Moore Foundation, the Canada Foundation for Innovation, the Ontario Ministry of Research and Innovation, the National Research Council of Canada, the Natural Sciences and Engineering Research Council of Canada, the British Columbia Knowledge Development Fund, the Association of Universities for Research in Astronomy (AURA) and the U.S. National Science Foundation.

A portion of the research in this paper was carried out at the Jet Propulsion Laboratory, California Institute of Technology, under a contract with the National Aeronautics and Space Administration.

REFERENCES

1. Aubrun, J.-N., Lorell, K. R., Havas, T. W., and Henninger, W. C., "Performance Analysis of the Segment Alignment Control System for the Ten-Meter Telescope," *Automatica*, Vol. 24, No. 4, pp. 437–453, 1988.
2. Jared, R. C. *et al.*, "The W. M. Keck Telescope segmented primary mirror active control system," *Proc. SPIE Vol. 1236 Advanced Technology Optical Telescopes IV* (Barr, L. D., ed.), 1990, pp. 996–1008.
3. MacMynowski, D. G., Blaurock, C., and Angeli, G. Z., "Dynamic Analysis of TMT," *Proc. SPIE*, 2008. SPIE 7017-31.
4. MacMynowski, D. G., Colavita, M. M., Skidmore, W., and Vogiatzis, K., "Primary mirror dynamic disturbance models for TMT: Vibration and wind," *Proc. SPIE 7738*, 2010.
5. Balas, M. J., "Trends in Large Space Structure Control Theory: Fondest Hopes, Wildest Dreams," *IEEE Trans. on Automatic Control*, Vol. 27, No. 3, pp. 522–535, 1982.
6. Aubrun, J.-N. and Lorell, K. R., "The Multi-Loop Control/Structure Interaction Effect: experimental verification using the ASCIE test bed," *NASA/DoD CSI Conference*, Nov 1990.
7. MacMynowski, D. G., Thompson, P. M., and Sirota, M. J., "Analysis of TMT Primary Mirror Control-Structure Interaction," *Proc. SPIE*, 2008. SPIE 7017-41.
8. MacMynowski, D. G., Thompson, P. M., and Sirota, M. J., "Control of many coupled oscillators and application to segmented-mirror telescopes," *AIAA Guidance, Navigation and Control Conference*, 2008.
9. Dimmler, M., Erm, T., Bauvir, B., Sedghi, B., Bonnet, H., Müller, M., and Wallander, A., "E-ELT Primary Mirror Control System," *Proc. SPIE Vol. 7012*, 2008.
10. Preumont, A., Bastaits, R., and Rodrigues, G., "Scale effects in active optics of large segmented mirrors," *Mechatronics*, Vol. 19, No. 8, pp. 1286–1293, 2009.
11. Chanan, G., MacMartin, D. G., Nelson, J., and Mast, T., "Control and Alignment of Segmented-Mirror Telescopes: Matrices, Modes, and Error Propagation," *Applied Optics*, Vol. 43, No. 6, pp. 1223–1232, 2004.
12. MacMynowski, D. G., "Interaction matrix uncertainty in active (and adaptive) optics," *Applied Optics*, Vol. 48, No. 11, pp. 2105–2114, 2009.
13. Thompson, P. M., MacMynowski, D. G., Colavita, M. M., Regehr, M. W., and Sirota, M. J., "Servo design and analysis for the Thirty Meter Telescope primary mirror actuators," *SPIE Vol. 7733*, 2010.
14. Doyle, J. C., Francis, B. A., and Tannenbaum, A. R., *Feedback Control Theory*, MacMillan, 1992.